doi.org/10.1002/cbdv.202201089

RESEARCH ARTICLE

CHEMISTRY & BIODIVERSITY

Antiproliferative Noscapinoids Bearing an Amidothiadiazole Scaffold as Apoptosis Inducers: Design, Synthesis and Molecular Docking

Ravi Kumar Pedapati,[a, b] Pratyush Pragyandipta,[c] Naga Pranathi Abburi,[a, b] Nagaraju Chirra,[a, b] Srinivas Kantevari,*[a, b] and Pradeep K. Naik*[c]

[a] Fluoro and Agrochemicals Department, CSIR-Indian Institute of Chemical Technology, Hyderabad, 500007, India, e-mail: kantevari@iict.res.in

[b] Academy of Scientific and Innovative Research (AcSIR), Ghaziabad, 201002, India

[c] Center of Excellence in Natural Products and Therapeutics, Department of Biotechnology and Bioinformatics, Sambalpur University, Jyoti Vihar, Burla, Sambalpur768 019, Odisha, India, e-mail: pknaik1973@gmail.com; pknaik1973@suniv.ac.in

Noscapine an FDA-approved antitussive agent. With low cytotoxicity with higher concentrations, noscapine and its derivatives have been shown to have exceptional anticancer properties against a variety of cancer cell lines. In order to increase its potency, in this study, we synthesized a series of new amido-thiadiazol coupled noscapinoids and tested their cytotoxicity in vitro. All of the newly synthesised compounds demonstrated potent cytotoxic potential, with IC_{50} values ranging from 2.1 to 61.2 μM than the lead molecule, noscapine (IC_{50} value ranges from 31 to 65.5 μM) across all cell lines, without affecting normal cells (IC_{50} value is > 300 μM). Molecular docking of all these molecules with tubulin (PDB ID: 6Y6D, resolution 2.20 Å) also revealed better binding affinity (docking score range from −5.418 to −9.679 kcal/mol) compared to noscapine (docking score is −5.304 kcal/mol). One of the most promising synthetic derivatives **6aa** (IC_{50} value ranges from 2.5 to 7.3 μM) was found to bind tubulin with the highest binding affinity ($\Delta G_{binding}$ is −28.97 kcal/mol) and induced apoptosis in cancer cells more effectively.

Keywords: Noscapine, amido-thiadiazole, breast cancer, apoptosis, antiproliferative.

Introduction

Due to its capacity to penetrate and spread throughout the body, cancer continues to be one of the major causes of death worldwide. Lung and breast cancers rank first among the top five cancer types in terms of incidence and mortality, and they account for one-third of all cancer cases and fatalities worldwide.[1] Despite the fact that there are a number of licensed pharmaceuticals for the treatment of cancer, the majority of them have multidrug resistance,[2] lethal side effects, and low specificities, necessitating the development of novel anticancer medications[3] with various modes of action.

One of the most important gifts given to mankind by nature has been the array of natural products that possess curative or therapeutic properties.[4] Noscapine is one of the many naturally occurring substances that has been discovered to be efficient as an anticancer agent. Noscapine **1**,[5,6] formerly known as narcotine, is a natural phthalide isoquinoline alkaloid that accounts for 7% of opium alkaloids. Noscapine has antitussive properties as well as a high safety profile. Despite being discovered from opium (*Papaver somniferum*) in 1817, this phthalideisoquinoline alkaloid has remained largely underrated in terms of therapeutic potential until Joshi et al.[7] discovered its antitumor activity. Noscapine, a tubulin-binding substance, was shown to stop cancer cells in their mitosis and cause apoptosis.[8] Contrary to taxanes, noscapine does not over polymerize or depolymerize tubulin (vincas). In contrast, it delicately attenuates micro-

Supporting information for this article is available on the WWW under https://doi.org/10.1002/cbdv.202201089

tubule dynamics and activates the mitotic checkpoints to bring the cell cycle to a halt, allowing other processes reliant upon less dynamic microtubules, such as axonal transport.[8–10] Because of this unique action, it is devoid of any severe toxicity. In contrast, due to the extreme effect on the microtubule, both taxanes and vincas cause severe toxicities such as leukocytopenia, diarrhoea, alopecia and peripheral neuropathies.[11–14] Clinical studies have demonstrated that noscapine and its derivatives can suppress the growth of cancer cells originating from various tissues and shrink implanted tumors in animals without causing any noticeable side effects.[8,15,16] Moreover, it retains activity against cancer cell lines resistant to paclitaxel (1 A9/PTX10, 1 A9/PTX22) and epothilone (1 A9/A8).[17] Further, it has favourable pharmacokinetic properties (clearance in 6–10 h).[18] All these worthy features of noscapine over the currently used chemotherapeutics raised tremendous hope for its potential use as a therapeutic compound and its further development in improving the potency.[19–21] In an effort to increase its anticancer effectiveness, we used rational drug design and chemical synthesis to create a variety of noscapinoids (*Figure 1*) that are currently undergoing various stages of chemical and biological evaluation.[22–26]

Additionally, compounds with a thiadiazole ring are well-known for their outstanding in vitro anticancer properties.[27] In the literature, there have been several compounds containing thiadiazole that have demonstrated excellent antitumor activities. As well, thiadiazole heteroatoms are capable of forming interactions with biological targets, such as hydrogen bonds. Kumar et al.[28] reported 1,3,4-thiadiazole-constructed compounds (i–v), there has been strong anticancer activity observed against several cancer cell lines, for instance LnCap, DU145, PC3, MCF-7, MDAMB-231, also PaCa2,[29] having IC_{50} values that range from 4.3 to 9.2 μM, and high choosiness (*Figure 2*). Kong et al.[30] In their work, developed a class of compounds that contained a 1,3,4-thiadiazole part. In their studies, compound (vi) demonstrated powerful activity against a number of cancer cell lines, including HepG2 cells for hepatocarcinoma ($IC_{50} = 6.6 \pm 2.2$ μM), A549 cells for non-small-cell lung cancer ($IC_{50} = 9.9 \pm 0.5$ μM), and MCF-7 cells for breast cancer ($IC_{50} = 11.8 \pm 0.6$ μM).

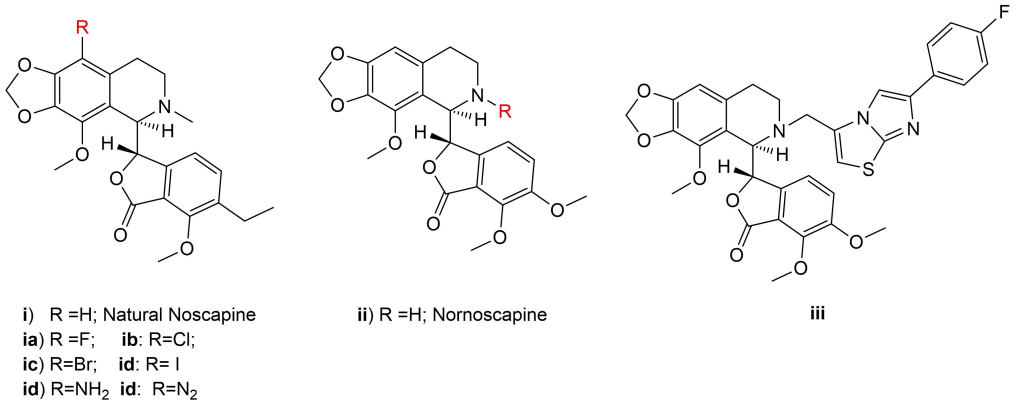

Figure 1. Potential cancer-fighting analogs of natural α-noscapine.

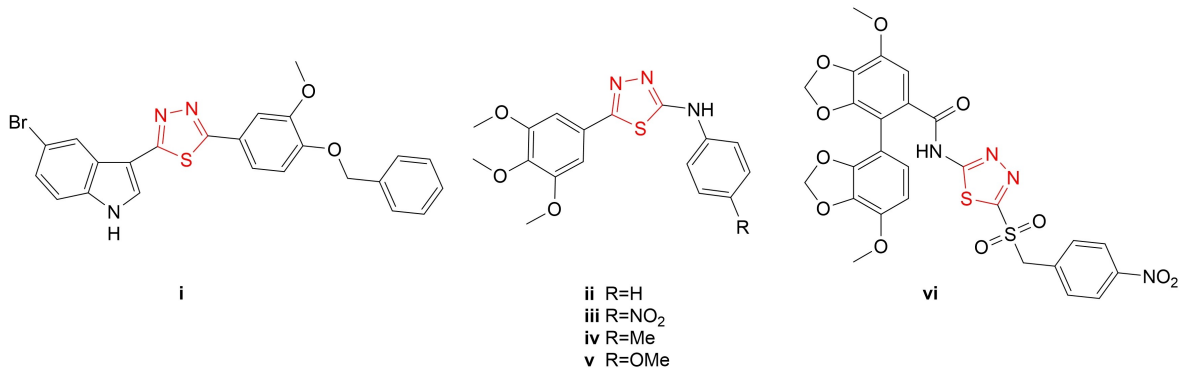

Figure 2. Examples of anticancer agents containing 1,3,4-thiadiazole group.

Our goal in this study has been to strategically change the scaffold of noscapine to create novel derivatives. These derivatives were then chemically synthesized and a biological investigation using a panel of human cancer cell lines of different tissue origin confirmed their anticancer activity. The newly synthesized derivatives were discovered to bind tubulin heterodimer with improved binding affinity, effectively suppress cancer cell proliferation, and successfully trigger apoptosis in cancer cells.

Results and Discussion

Chemistry

Natural noscapine **1** was undergone *O*-demethylation with NaN_3 and NaI in DMF at 135–140 °C to give compound **2** (**Nos**–**OH**) in 78% yield.[31] We then used K_2CO_3 as a base in a reaction with 1,4-dibromobutane in acetone at reflux for 4 h to produce compound **3** from Nos–OH (**2**) in 92% yield.

Noscapinoid **3** was further treated with 5-amino-1,3,4-thiadiazole-2-thiol in DMF using K_2CO_3 as a base at 80 °C for 2h to produce compound **4** in 82% yield. Noscapinoid **4** was further converted to **6a**–**6ac** by reacting with substituted benzoic acids **5a**–**5ac** in DCM at 50 °C for 15h in the presence of EDC.HCL, HOBt, and Et_3N as a base (*Scheme 1* and *2*)). Following the completion of the reaction, which was monitored using TLC, the mixture was separated into aqueous and organic layers. The organic layer was then collected, evaporated under a vacuum, and done flash chromatography over silica gel with hexane/ethyl acetate (7:3), yielding the anticipated noscapinoids **6a**–**6ac** (*Figure 3*). All the products **2**, **3**, **4** and **6a**–**6ac** were analyzed by ^1H & ^{13}C-NMR and Mass (ESI and HRMS) spectral data (*Supporting Information*). For instance, the ^1H-NMR spectrum of **6j** showed amide specific proton as a singlet at δ 10.80 (1H). The aromatic protons were observed at δ 7.97 (2H), δ 6.92 (1H), δ 6.72 (2H), δ 6.05 (1H) as doublets, and δ 6.30 (1H) as a singlet. C–C bridged protons (in between Phthalide and isoquinoline) of noscapine appeared at δ 5.56 (1H) and δ 4.38 (1H) as doublets and methylenedioxy protons observed at δ 5.93 (2H) as a doublet of doublet, and two methoxy groups of

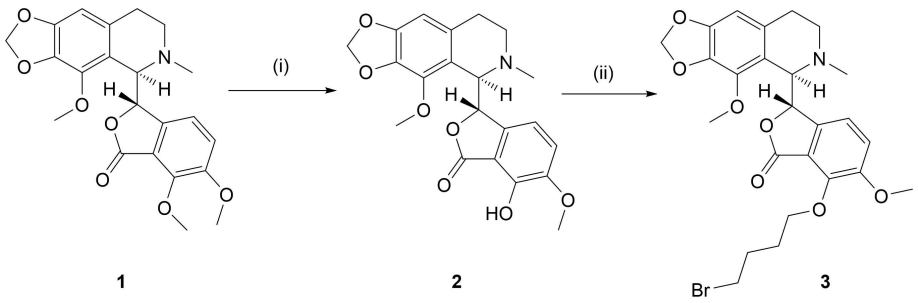

Scheme 1. Synthesis of compound **3**. Reaction conditions: (i) NaN_3, NaI, DMF, 140 °C, 4h, 78%, (ii) 1,4-dibromobutane, K_2CO_3, KI, acetone, reflux, 4h, 92%.

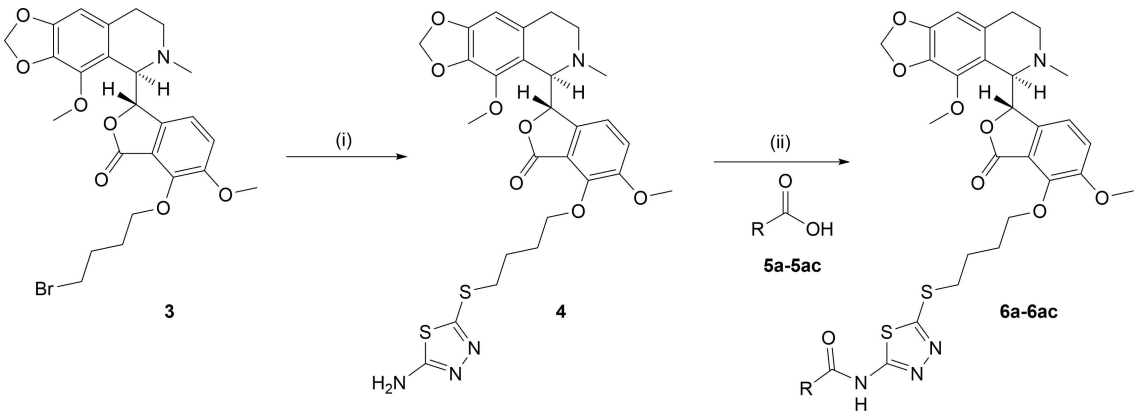

Scheme 2. Synthesis of amido thiazole coupled noscapinoids (**6a**–**6ac**). Reaction conditions: (i) 5-amino-1,3,4-thiadiazole-2-thiol, K_2CO_3, DMF, 80 °C, 2h, 82%, (ii) **5a**–**ac**, EDC.HCL, HOBT, Et_3N, Dry DCM, 50 °C, 15h, 43–94%.

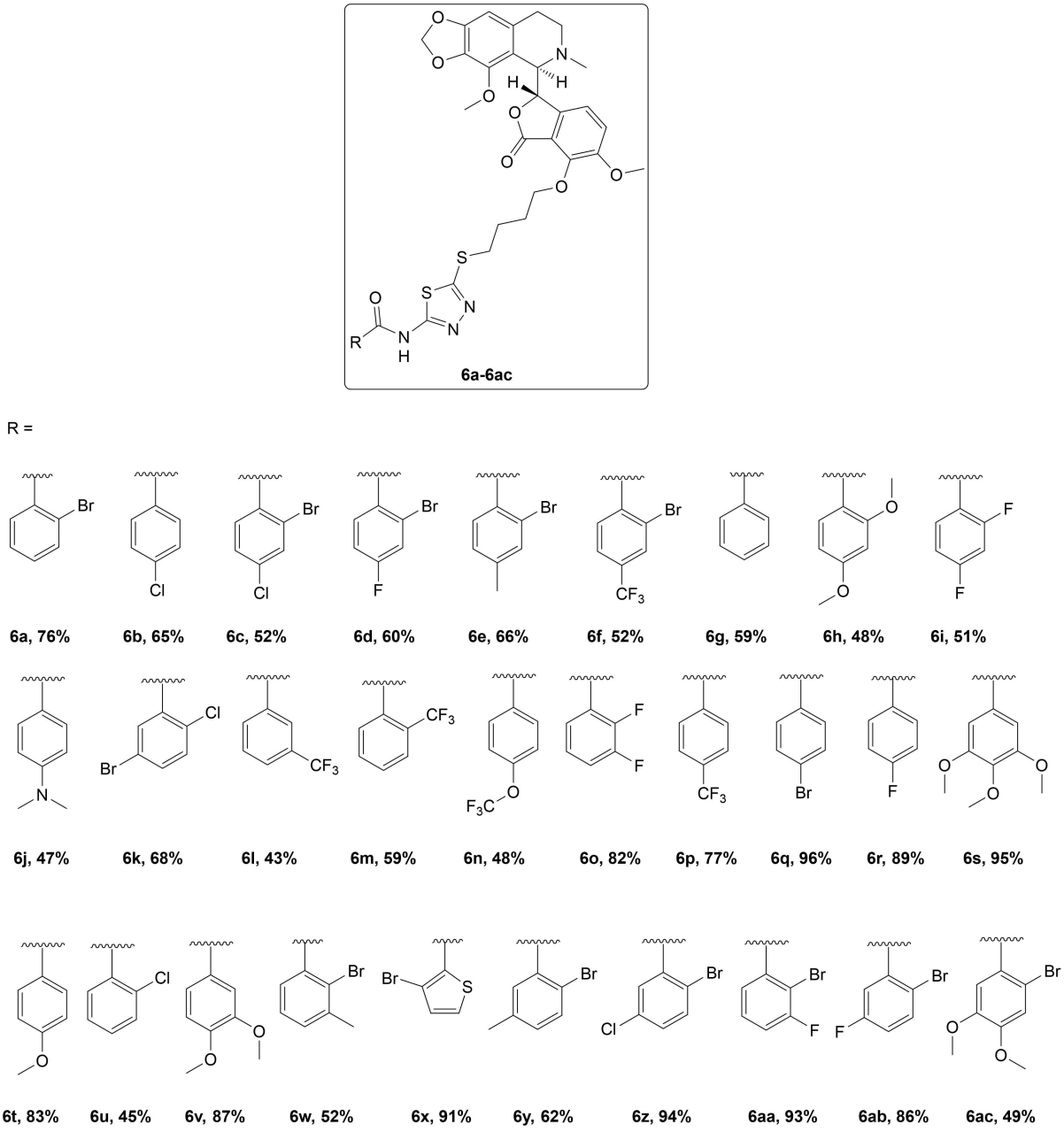

Figure 3. Library of synthesized substituted amido-thiadiazole coupled noscapinoids (**6a**–**6ac**).

noscapine observed at δ 4.03 (3H), δ 3.81 (3H), as singlets. And the –O–CH_2– protons present in the linker were observed as a multiplet at δ 4.30–4.20 (2H). Characteristic –S–CH_2– protons in the linker appeared at δ 3.37 (2H) as a triplet. And the characteristic –$N(CH_3)_2$ protons appeared as a singlet at δ 3.08 (6H). The remaining N–CH_3 protons and the aliphatic protons of the linker and the isoquinoline group fall under the range of 2.62–1.83 as multiplets respectively (supporting info). HRMS of **6j** at *m/z* 734.23128 for $C_{36}H_{39}N_5O_8S_2$ $[M+H]+$ confirmed the molecular formula and the structure.

Biology

The natural lead chemical noscapine's capacity to kill cells was multiplied by the synthesis of numerous promising derivatives. Since many of these derivatives dissociation constants (K_d) were much lower than the noscapine's value of 152 μM, it was shown that many of them had higher free energies for binding to

tubulin. For instance, nitro noscapine has a K_d value of 86 μM and amino noscapine has a value of 14 μM, for the halogen derivatives which vary from 80 to 22 μM.[32–34] Additionally, by functionalizing 'N' in the isoquinoline moiety of natural α-noscapine and connecting biaryl pharmacophore,[26] we have created a library of derivatives. Additionally, compared to noscapine, all of these derivatives displayed a lower K_d value. In this study, we present a panel of amido-thiadiazole coupled noscapinoids that show promising tubulin-binding anticancer activity.

Cell Viability

Six different cancer cell lines with a variety of tissue origins were used to investigate the anti-proliferative activity of all the amido-thiadiazol linked noscapinoids **6a**–**6ac**, as well as the parent molecule noscapine. In comparison to noscapine, all of the amido-thiadiazol linked noscapinoids had strong cytotoxic activity. In *Table 1*, the IC_{50} values for the cell lines for amido-thiadiazol linked derivatives are compiled. Compared to untreated cells, the IC_{50} value of noscapine, and its amido-thiadiazole derivatives for cancer cell lines was shown to be statistically significant ($p < 0.05$). Surprisingly noscapine and the synthesized derivatives inhibited the proliferation of normal healthy cells with

Table 1. IC_{50} values (in μM range) calculated based on three biological repeats for amido-thiadiazol coupled noscapinoids (**6a**–**6ac**) using cancer cell lines as well as a normal cell lines (HEK). It was discovered that all of the new derivatives had improved antiproliferative activity in comparison to noscapine. Using the student t-test, it was determined that the IC_{50} values between treated and untreated cells were statistically significant ($p < 0.05$).

S No.	Compound	IC_{50}(μM) ± SD						
		MCF-7 (Breast cancer)	MDAMB-231 (Breast cancer)	SAOS (osteosarcoma)	h-1299 (Lung cancer)	Hep–G2 (Liver cancer)	HeLa (Cervical cancer)	HEK (Embryonic kidney cell lines)
1	Noscapine (**1**)	43.9 ± 4.6	60.9 ± 3.8	65.5 ± 4.3	59.2 ± 4.8	34.7 ± 3.2	31 ± 3.5	312.6 ± 2.2
2	**6a**	7.2 ± 2.0	15 ± 1.2	12 ± 1.6	7 ± 2.2	5 ± 1.3	15 ± 1.1	340.1 ± 9.6
3	**6b**	15.5 ± 1.7	35.5 ± 1.4	28.2 ± 2.9	12 ± 3.1	15 ± 2.2	22 ± 1.8	342.1 ± 11.2
4	**6c**	9.5 ± 1.7	12.5 ± 1.7	11 ± 2.7	12 ± 3.4	8.5 ± 1.8	14 ± 0.8	338.6 ± 12.0
5	**6d**	41 ± 1.4	61.2 ± 2.6	52.5 ± 3.9	42 ± 3.6	37 ± 2.4	39 ± 2.2	338.9 ± 19.0
6	**6e**	20 ± 1.3	35.4 ± 2.0	25.7 ± 4.4	23 ± 2.4	19 ± 1.2	25 ± 3.2	339.5 ± 16.5
7	**6f**	25 ± 1.3	42.5 ± 2.3	32.8 ± 4.1	22 ± 2.2	14 ± 1.1	26 ± 2.2	343.0 ± 9.2
8	**6g**	18 ± 1.2	30.1 ± 3.2	25 ± 3.4	24 ± 2.4	25.2 ± 2.4	31.5 ± 3.1	343.0 ± 12.5
9	**6h**	20 ± 0.8	33.2 ± 2.7	28.5 ± 5.7	24.5 ± 1.7	17.4 ± 2.2	22 ± 3.6	341.2 ± 9.6
10	**6i**	19.5 ± 2.1	30.3 ± 2.5	25 ± 2.3	18.4 ± 2.5	15.2 ± 3.5	19 ± 2.1	342.4 ± 4.7
11	**6j**	23.7 ± 2.1	31.5 ± 1.9	27.1 ± 2.5	32 ± 2.6	25 ± 2.2	23.8 ± 3.2	335.7 ± 13.5
12	**6k**	12 ± 1.7	20.3 ± 1.6	15.3 ± 2.9	14 ± 2.3	12.5 ± 1.9	16.2 ± 1.2	338.3 ± 7.8
13	**6l**	10.5 ± 1.8	16.8 ± 2.5	12.3 ± 1.9	12.7 ± 2.5	15.6 ± 1.9	19.4 ± 2.5	344.9 ± 12.5
14	**6m**	12.3 ± 1.1	20.2 ± 1.5	15 ± 2.3	12.9 ± 1.4	10.5 ± 1.1	13.5 ± 2.9	347.3 ± 13.5
15	**6n**	4.5 ± 0.7	7.6 ± 1.8	6.6 ± 2.0	8.5 ± 2.8	4.5 ± 0.8	7.5 ± 1.5	315.6 ± 2.5
16	**6o**	5.9 ± 0.3	10.9 ± 3.1	8 ± 1.7	9.6 ± 2.1	4.5 ± 0.9	6.5 ± 1.6	336.2 ± 7.2
17	**6p**	7.5 ± 0.7	14.2 ± 2.7	9.5 ± 3.1	10.5 ± 2.1	4.3 ± 0.8	12.4 ± 1.7	344.4 ± 2.6
18	**6q**	15.5 ± 1.8	25.9 ± 3.3	20 ± 2.1	7.5 ± 1.6	5.5 ± 0.7	7.9 ± 1.1	354.4 ± 3.8
19	**6r**	37.1 ± 1.2	47.4 ± 3.6	35.5 ± 3.1	40.7 ± 3.9	30.3 ± 2.4	34.5 ± 4.1	349.6 ± 8.7
20	**6s**	25 ± 1.4	45.6 ± 3.0	30 ± 3.6	32.5v2.8	22.7 ± 2.3	30.3 ± 1.7	358.1 ± 5.2
21	**6t**	20 ± 1.6	32.4 ± 2.7	26 ± 2.3	30.5 ± 1.9	26.3 ± 2.5	33.4 ± 2.7	347.4 ± 3.9
22	**6u**	32.6 ± 1.1	45.8 ± 2.2	37 ± 3.1	24.3 ± 3.0	22.5 ± 3.1	34.2 ± 2.3	343.1 ± 11.3
23	**6v**	20.9 ± 2.5	35.3 ± 2.6	23v2.4	38.5 ± 3.9	25.2 ± 3.6	14.3 ± 1.8	345.5 ± 10.7
24	**6w**	38.4 ± 2.0	54.6 ± 2.8	43 ± 2.2	44.5 ± 2.8	34.2 ± 4.0	42.4 ± 3.8	339.3 ± 11.2
25	**6x**	27.5 ± 1.7	46.3 ± 2.7	32 ± 2.8	32.5 ± 3.9	33.5 ± 3.7	43.3 ± 2.5	339.5 ± 7.2
26	**6y**	20 ± 1.6	31.7 ± 3.3	27 ± 2.7	32.3 ± 3.7	16.4 ± 2.2	22.4 ± 1.5	339.4 ± 9.8
27	**6z**	17.5 ± 1.9	29.6 ± 2.3	22 ± 2.2	24.6 ± 3.0	14.5 ± 2.6	22.5 ± 2.8	337.5 ± 8.7
28	**6aa**	2.5 ± 0.2	6.5 ± 1.2	4.5 ± 0.7	5.8 ± 2.4	2.1 ± 0.3	7.3 ± 1.0	341.4 ± 6.4
29	**6ab**	31.4 ± 1.7	44.7 ± 2.8	37.5 ± 2.6	33.8 ± 4.2	28.9 ± 3.3	36.9 ± 6.0	339.8 ± 8.3
30	**6ac**	27.3 ± 0.8	47.2 ± 3.7	35 ± 2.3	39.7 ± 4.3	28.5 ± 3.7	43.8 ± 5.3	340.5 ± 7.7

IC_{50} value > 300 μM, indicating that these compounds were not toxic to normal HEK cell lines (*Table 1*). Among the amido-thiadiazole coupled noscapinoids **6n** and **6aa** showed promising antiproliferative activity using all the cell lines (*Table 1*). The compound 6aa was selected for the detailed investigation.

Apoptosis Assay

The primary morphological changes that occur during apoptosis usually include membrane blebbing, cellular shrinkage, chromatin condensation, and the creation of apoptotic bodies. Consequently, we engaged in cellular studies using AO, EtBr and HO (Hoechst 33342) to confirm the induction of apoptosis by one of the most promising derivatives **6aa** using MDAMB-231 breast cancer cell lines. The treated cells underwent apoptosis as demonstrated by the staining of the treated cells with these dyes (*Figure 4*). Specifically, the untreated cells were observed to have normal cell morphology. In contrast, the treated cells underwent several features of apoptosis such as membrane blebbing, numerous fragmented nuclei, and the appearance of apoptotic bodies.

Effects of the Compound **6aa** *on ROS Accumulation in MDAMB-231 Cells*

To learn more about the process by which cancer cells induce apoptosis, we found that treatment with noscapinoid **6aa** elevated ROS levels in cancer cells. Using DCFDA as the molecular probe, the ROS level was analyzed using MDAMB-231 cells treated with **6aa**. Compound **6aa** treatment increased the red fluorescence in MDAMB-231 cells compared to untreated cells (*Figure 5*). We found that compound **6aa** significantly elevated ROS levels in MDAMB-231 cells

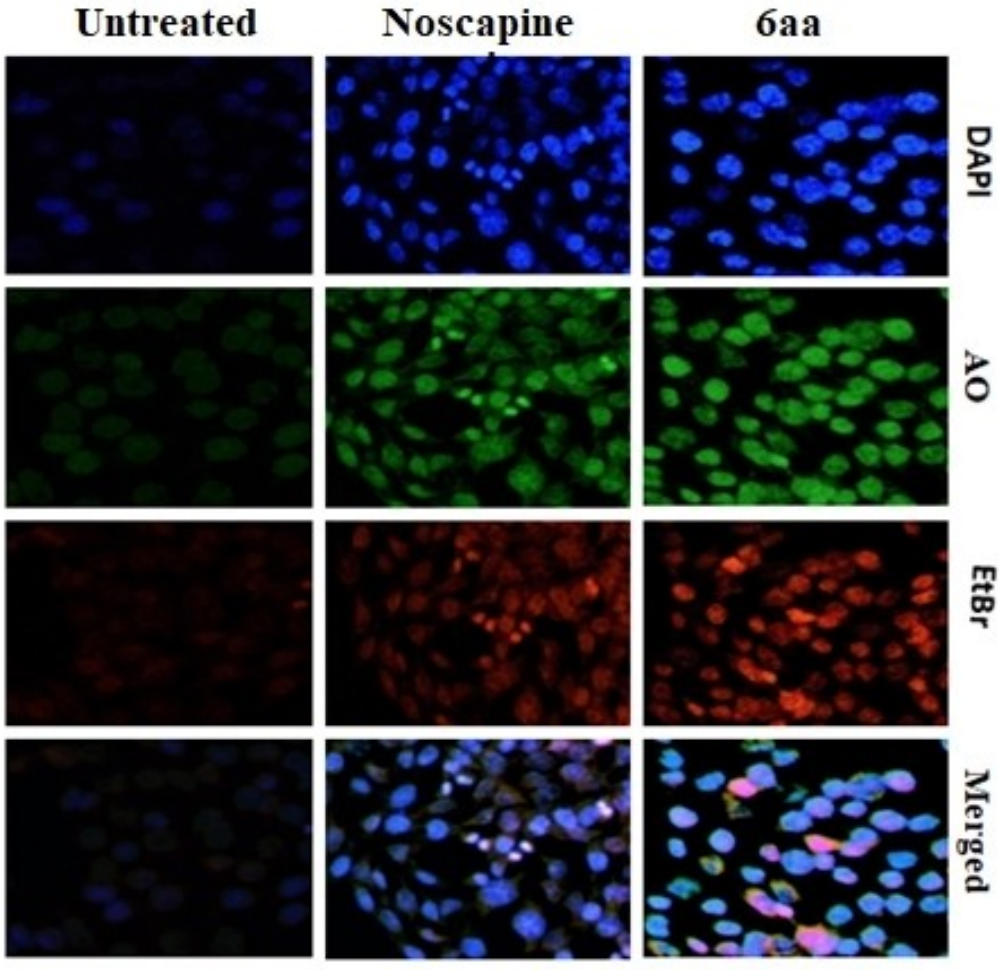

Figure 4. Induction of apoptosis by the most promising derivative **6aa**. Morphological changes of MDAMB-231 cells visualized by staining with DAPI, AO, EtBr and merged revealed apoptosis with the treatment of **6aa** compared to untreated cells.

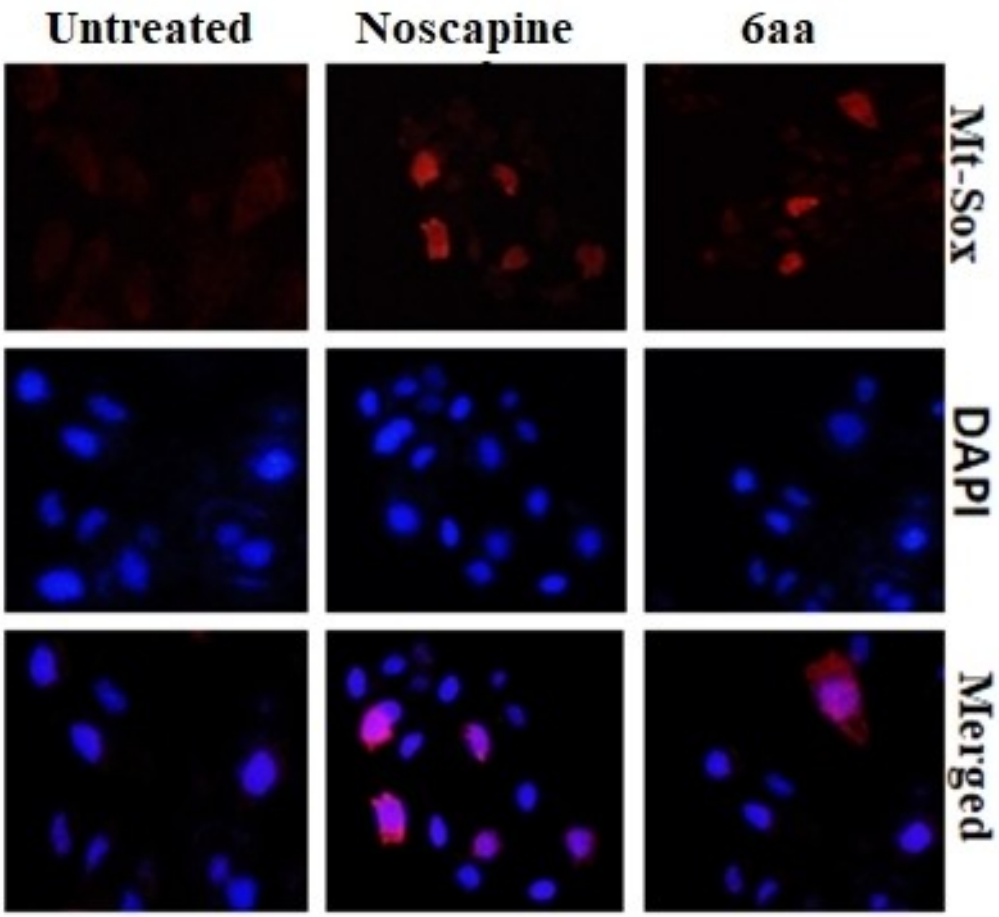

Figure 5. Treatment with compound **6aa** at its IC_{50} concentration (7.6 μM) increases the ROS level in MDAMB-231 cells compared to untreated cells as measured by the fluorescent dye DCFDA.

as measured by fluorescent intensity, indicating that ROS might have a role in inducing apoptosis.

Effects of Compound **6aa** *on Mitochondrial Membrane Potential (ΔΨm)*

Apoptosis is assumed to primarily occur through mitochondria. The induction of apoptosis is closely related to the collapse of mitochondrial membrane potential ($\Delta\Psi$m). Thus, we have measured the loss of mitochondrial membrane potential ($\Delta\Psi$m) in MDAMB-231 cells treated with compound **6aa** using DAPI, JC-1, and Rhodamine 123 dyes. When compound **6aa** was used to treat MDA-MB-231 cells, JC-1(red fluorescence), Rhodamine-123 (green fluorescence), and DAPI (blue fluorescence) in treated cells were more intense compared to untreated cells (*Figure 6*). Comparing treated and untreated MDAMB-231 cells, compound **6aa** dramatically exacerbated the loss of mitochondrial membrane potential ($\Delta\Psi$m).

Molecular Docking

The noscapine and its synthesized analogs were docked using Glide XP onto the noscapinoid binding site[35] at the interface between α- and β-tubulin. All these molecules were found to fit nicely inside the binding site. Their binding affinity with tubulin is also assessed using Glide XP_{score} function.[36,37] Compared to noscapine (docking score is −5.304 kcal/mol), the synthesized analogs showed superior docking scores of −5.418 to −9.679 kcal/mol (*Table 2*). The docked complex of one of the most promising derivatives **6aa** with tubulin was considered for MD simulation of 100 ns to examine the stability of the complex. Plotting the root mean square deviation (RMSD) of the backbone C_α atoms with respect to time allowed for

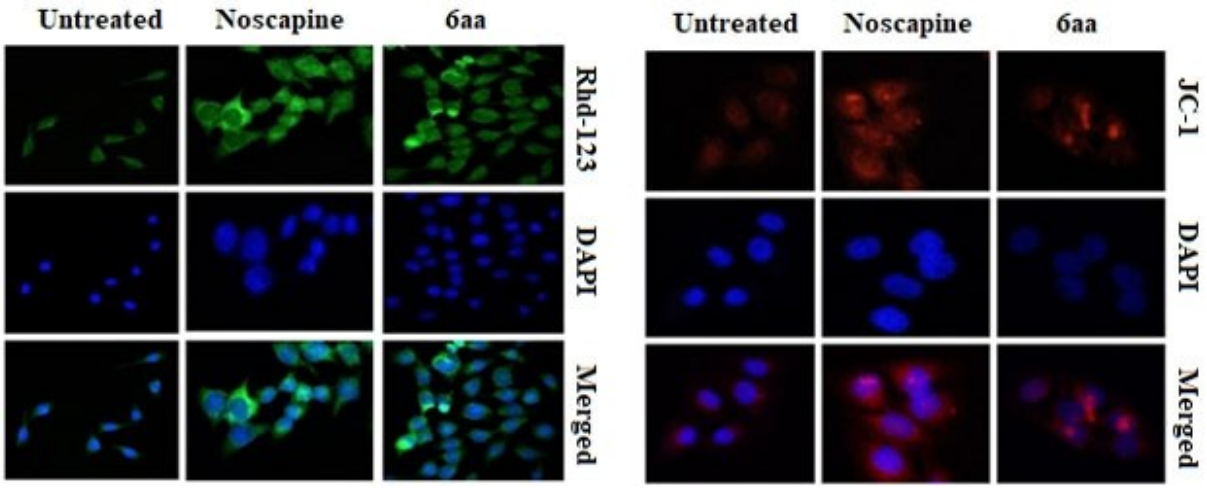

Figure 6. Effect of compound **6aa** on mitochondrial membrane potential as visualized using different fluorescent dyes, DAPI, JC–I, Rhodamine 123 and merging of both the dyes.

Table 2. Results of molecular docking of amido-thiadiazol coupled noscapinoids (**6a**–**6ac**) with tubulin. All the molecules were found to be docked well within the binding site with high binding affinity compared to the lead molecule, noscapine.

Sl No.	Ligands	Glide gscore (kcal/mol)	Glide lipo (kcal/mol)	Glide Evdw (kcal/mol)	Glide Ecoul (kcal/mol)	Glide Emodel (kcal/mol)	Glide energy (kcal/mol)
1	Noscapine (**1**)	−5.304	−0.589	−7.858	−20.456	−43.032	5.726
2	**6a**	−6.528	−4.251	−57.284	−8.272	−88.336	−65.557
3	**6b**	−5.933	−3.731	−58.200	−7.615	−97.483	−65.815
4	**6c**	−6.849	−4.645	−58.714	−8.862	−91.274	−67.576
5	**6d**	−6.165	−4.666	−45.500	−8.573	−85.105	−54.073
6	**6e**	−6.579	−4.856	−58.714	−8.012	−87.274	−66.726
7	**6f**	−7.417	−4.564	−59.681	−8.392	−87.656	−68.074
8	**6g**	−6.478	−3.133	−47.969	−9.769	−88.634	−57.738
9	**6h**	−6.673	−4.189	−58.295	−11.122	−83.399	−69.417
10	**6i**	−6.947	−3.367	−50.892	−9.199	−86.048	−60.091
11	**6j**	−7.432	−3.965	−48.008	−9.693	−84.755	−57.702
12	**6k**	−6.775	−4.349	−56.535	−8.831	−74.128	−65.366
13	**6l**	−8.253	−4.765	−44.289	−3.385	−21.283	−47.674
14	**6m**	−6.586	−4.598	−57.080	−5.663	−84.925	−62.744
15	**6n**	−6.947	−4.153	−63.278	−9.088	−99.968	−72.366
16	**6o**	−6.787	−4.406	−62.697	−5.272	−92.220	−67.969
17	**6p**	−7.527	−3.471	−47.898	−9.380	−78.033	−57.278
18	**6q**	−6.348	−4.628	−57.483	−11.096	−74.736	−68.579
19	**6r**	−7.946	−7.776	−66.925	−3.787	−88.444	−70.712
20	**6s**	−5.418	−5.143	−62.075	−9.097	−88.054	−71.172
21	**6t**	−6.704	−3.984	−53.198	−8.074	−73.807	−61.272
22	**6u**	−6.244	−3.611	−52.396	−12.041	−83.675	−64.437
23	**6v**	−9.196	−7.079	−55.823	−8.767	−95.114	−64.591
24	**6w**	−6.568	−4.646	−55.526	−5.491	−81.241	−61.017
25	**6x**	−5.609	−3.653	−55.004	−6.905	−88.079	−61.909
26	**6y**	−6.611	−4.630	−51.666	−7.306	−62.947	−58.972
27	**6z**	−6.675	−5.007	−62.812	−4.086	−94.295	−66.898
28	**6aa**	−9.679	−5.991	−64.808	−13.085	−113.016	−77.893
29	**6ab**	−6.833	−4.549	−59.740	−6.921	−69.280	−66.661
30	**6ac**	−5.694	−4.064	−51.409	−8.425	−66.459	−59.834

the observation of the convergence of the MD trajectories. The relative fluctuation of the RMSD (< 0.5 Å) was minimal, suggesting the system's stability. Furthermore, to determine how flexible these residues are, the root mean square fluctuations (RMSF) of the bound and free forms of the tubulin residues were calculated. For both α- and β-tubulin, the RMSF values of the residues in the bound and free forms were observed to be minimal (< 4 Å), indicating that the residues were more rigid. Overall, the compound **6aa** was well housed inside the binding site, at the interface between α- and β-tubulin (*Figure 7 C&D*). Five hydrogen bonds were formed between **6aa** and the amino acids at the binding site. In addition to hydrogen bonds, a significant number of hydrophobic interactions were implicated in its binding with the residues in the binding site (*Figure 7E*).

The Compound **6aa** *Revealed High Free Energy of Binding with Tubulin*

The assumptive binding free energy ($\Delta G_{bind,PB(GB)}$) of natural noscapine and its most promising amido-thiadiazole coupled derivative (**6aa**) with tubulin according to MM-PBSA is compiled in *Table 3*. The binding free energy (ΔG_{bind}) and its components for noscapine and **6aa** were determined as the mean value from 500 snapshots obtained from the final 10 ns of the MD trajectory. Comparing compound **6aa** to noscapine, it was shown that compound **6aa** has a higher binding affinity for tubulin. It showed the highest binding energy of −28.97 kcal/mol. Both the intermolecular van der Waals (ΔE_{vdw}) and the electrostatic (ΔE_{ele}) interactions contributed significantly to the binding, whereas the polar solvation terms (ΔG_{polar}) inhibit binding. On the other hand, solvent accessible surface area terms (ΔG_{SASA}), had minimal contribution.

Table 3. Binding free energy and its components (kcal/mol) calculated for the noscapine and one of its most promising derivatives **6aa** with αβ tubulin dimer.

Complex	ΔE_{elec} Kcal/mol	ΔE_{vdw} Kcal/mol	ΔG_{polar} Kcal/mol	ΔG_{SASA} Kcal/mol	$\Delta G_{binding}$ Kcal/mol
Noscapine	−46.34	−18.23	46.48	−4.85	−22.94
6aa	−52.81	−20.42	49.28	−5.02	−28.97

Predicted ADME Properties of Noscapine and its Newly Synthesized Analogs

With the aid of QikProp (Schrodinger software package), we have evaluated the absorption, distribution, metabolism, and excretion (ADME) characteristics of noscapine and its amido-thiadiazol linked derivatives. Several ADME properties such as molecular weight (MW), total solvent accessible surface area (SASA), octanol/water partition coefficient (QPlogPo/w), octanol/gas partition coefficient (QPlogPoct), water/gas partition coefficient (QPlogPw), polarizability in cubic angstroms (QPlogrz), % human oral absorption in intestine (QP%), brain/blood partition coefficient (QPlogBB), IC_{50} value for blockage of HERG K+ channel (QPlogHERG), skin permeability (QPlogKp), prediction of binding to human serum albumin (QPlogKhsa), apparent Caco-2 cell permeability in nm/sec (QPPCaco) and apparent MDCK cell permeability in nm/sec (QPPMDCK) were predicted. While MDCK cells are thought to be an excellent mimic for the blood-brain barrier, Caco-2 cells serve as a model for the gut-blood barrier. Also, we assessed the acceptance level of noscapine and its new synthetic analogs using Lipinski's rule of five (number of violations of Lipinski's rule of five), which is crucial for rational drug design. It was fascinating to know that noscapine and its amido-thiadiazol coupled derivatives showed significant values for the properties studied and qualified all of the drug-like properties using Lipinski's rule of 5 (*Table 4*).

Conclusion

In conclusion, to hasten the anticancer activity of the natural lead molecule noscapine, we have carefully constructed a panel of amido-thiadiazol coupled noscapinoids. We have also provided the most straightforward methods for the direct modification of the noscapine scaffold to produce the amido-thiadiazol coupled noscapinoids in high yields. Based on our detailed molecular modelling and cellular analysis employing several cancer cell lines, all the derivatives generated have demonstrated improved antiproliferative activity to cancer cells without damaging normal healthy cells. As a result, these compounds may prove effective in treating other malignancies in addition to breast cancer. Our findings encourage us to keep investigating how these novel substances affect *in vivo* animal tests with the ultimate objective of applying it to a clinical study on humans.

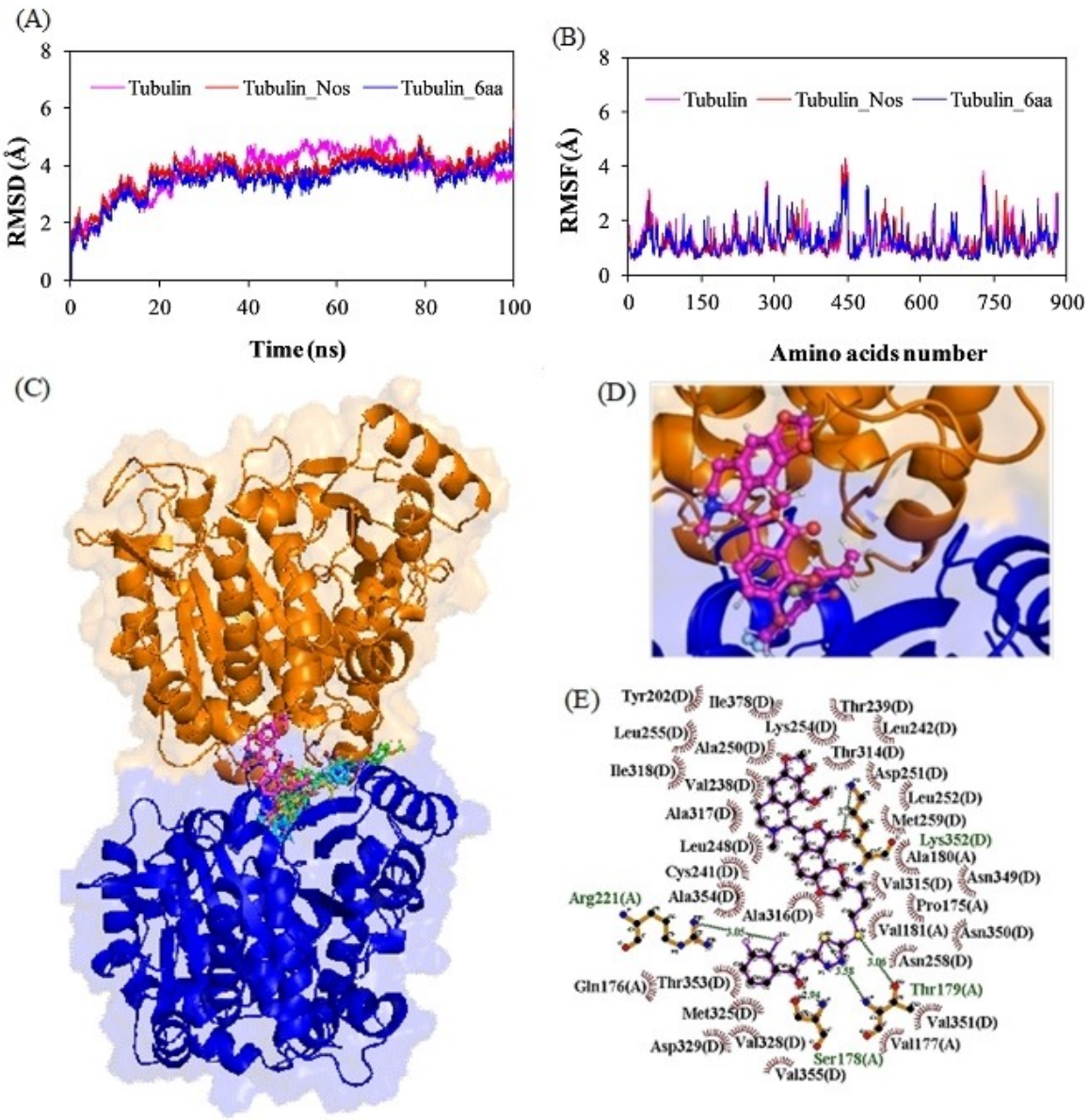

Figure 7. Molecular modeling evaluation of the binding of amido-thiadiazol coupled noscapinoids (**6a**–**6ac**) onto tubulin. (A) Root mean square deviations (RMSD) of Cα carbon atoms of tubulin only and in complex with compound **6aa** during 100 ns of MD simulation. The relative fluctuation in the RMSD of the Cα atoms is very small (<0.5 Å) for the entire duration of the simulation, indicating stability of the system. (B) Root mean square fluctuation (RMSF) of the residues in the bound form and in the unbound form of tubulin heterodimer. Different levels of flexibility of these residues were noticed in the free and bound form of tubulin with ligands. All the amino acids showed very low fluctuation (<4.0 Å) indicating that most of the residues were rigid both in free and bound form of tubulin. (C) Amido-thiadiazol coupled noscapinoids (**6a**–**6ac**) bind to tubulin at the interface of α- and β- tubulin (α-tubulin is displayed in brown color and β-tubulin is displayed in blue). (D) The most promising compound **6aa** fits comfortably into the noscapine binding site at the interface of tubulins α- and β. (E) Two-dimensional illustration of interaction detected between the binding site residues of tubulin and the compound **6aa**. Five hydrogen bonds were involved in the binding of **6aa** with the binding site amino acids.

Table 4. A list of characteristics determined by Qikprop simulation for Noscapine and its promising amido-thiadiazole coupled derivative **6aa** for the ADME screening. In this investigation, it was discovered that noscapine and its new synthetic analog **6aa** met every requirement for ADME screening.

Sl No.	ADME Screening	**6aa**	Noscapine	Recommended values
1	MW.	587.67	413.43	130–725
2	SASA	724.61	597.91	300–1000
3	Accpt HB	13.25	8.75	2.0–20.0
4	QPpolrz	68.75	38.69	13.0–70.0
5	QPlogPoct	32.75	17.70	8.0–35
6	QPlogPw	16.99	10.15	4.0–45.0
7	QPlogPo/w	5.57	1.68	−2.0–6.5
8	QPlogHERG	−7.61	−4.53	Below −5.0
9	QPPCaco	143.62	661.79	<25 poor >500 great
10	QPlogBB	−0.87	0.27	−3.0–1.2
11	QPPMDCK	418.55	350.31	<25 poor >500 great
12	QPlogKp	−4.01	−4.09	−8.0–−1.0
13	QPlogKhsa	0.75	−0.52	−1.5–1.5
14	Rule of Five (No. of violations)	3.00	0.00	Maximum is 4

Experimental Section

Molecular Docking

Protein Preparation

The PDB (protein data bank) structure of tubulin (PDB ID: 6Y6D, resolution 2.20 Å)[35] was downloaded and used for the molecular modelling study. Although tubulin's crystal structure is generated at high resolution (2.20 Å), it has specific errors like missing hydrogen atoms, and missing side-chain atoms of some amino acids. The multistep procedure of protein preparation wizard (Schrödinger, Inc., NY) was used to add the missing hydrogen atoms. The missing side chain atoms of the amino acids were identified using the Prime side chain prediction tool and repaired using Prime (Schrödinger, Inc., NY). Furthermore, the structure was refined by energy minimization using Macromodel (Schrodinger) and OPLS 2005 force field. Polak-Ribiere Conjugate Gradient (PRCG) algorithm with an energy gradient of 0.01 kcal/mol was used for the energy minimization.

Preparation of Molecular Structures of Amido-Thiadiazole Coupled Noscapinoids

The newly designed derivatives of Noscapine (*Figure 2*) were built using Chemdraw. These molecular structures were energy minimized using Macromodel (Schrödinger package) and OPLS 2005 force field with PRCG algorithm (energy gradient of 0.001). The ligand structures were further refined by geometric optimization using hybrid density functional theory with Becke's three-parameter exchange potential and the Lee-Yang-Parr correlation functional (B3LYP) with basis set 3-21G* using Jaguar (Schrödinger, package). The various conformations of the ligands were generated using Ligprep (Schrödinger package).

Molecular Docking

The prepared structures of amido-thiadiazole coupled noscapinoids were docked with αβ-tubulin heterodimer using Glide (Schrödinger package) as reported previously.[38] Glide grid-receptor generation program was used to create a grid box of size 12 Å ×12 Å ×12 Å at the centroid of the co-crystal ligand, aminonoscapine. Noscapinoids were docked into the binding site using Glide XP (extra precision) and their binding poses were evaluated using a Glide XPScore function.[36,37] The single best conformation for each ligand was considered for further analysis.

Molecular Dynamics Simulation of Docked Complexes

Molecular dynamics (MD) simulation of one of the promising amido-thiadiazole coupled noscapinoids **6aa** with tubulin in the presence of GTP, GDP and magnesium was carried out using GROMACS 2019.2 package.[39] The docked conformation of the complex with the lowest minimum docking score was taken as the initial conformation for MD simulation. The protein was processed with AMBER 999SB force field[40] to

generate coordinates and topology files. Parameters for all the 3 ligands (GTP, GDP and compound **6aa**) were estimated using a general amber force field (GAFF)[41] implemented in the antechamber program of Amber 18. All atomic point charges were calculated using the AM1-BCC charge model.[42] Topologies and internal coordinates for all ligands were generated using the tleap program of Amber 18 and ACPYPE software.[43] The complex was solvated with a TIP3P water model in a truncated octahedron box with a distance of 12 Å between the atoms of protein and the wall of the box. Counter ions at physiological ionic strength (0.15 M) neutralized the system. Energy minimization was performed using the Steepest descent method of 10000 steps to release conflicting contacts. After applying position restraints of 10 kcal/Å^2 on protein and ligands, NVT equilibration of 500 ps run was done at 300 K, followed by NPT equilibration of 500 ps with Parrinello-Rahman barostat at a reference pressure of 1 bar. After equilibration, a production MD run was performed for 100 ns with a time step of 2 fs. Particle-mesh Ewald algorithm (PME) was used for long-range electrostatic interactions. Short-range electrostatics and van der Waals cut-offs were set at 10 Å. The bonds were constrained using a shake algorithm[44] and a modified Berendsen thermostat was used to regulate the temperature of the system. The atomic coordinates were recorded every 20 ps during the MD simulation. Gromacs tools were used to analyze trajectories for Root Mean Square Deviation (RMSD), Radius of gyration (Rg) and Root Mean Square Fluctuation (RMSF). All plots were generated using GRACE software. The complex with the lowest minimum total energy from the MD trajectory was used to elucidate the binding mode of the ligand.

Prediction of Binding Free Energy Using MM-PBSA Technique

The predicted binding free energy of the active compound **6aa** with tubulin was calculated based on Molecular Mechanics Poisson-Boltzmann Surface Area (MM-PBSA).[45] From the last 10 ns of MD trajectory, 500 snapshots were extracted with a time step of 20 ps and the ensemble average of the $\Delta G_{bind,PBSA}$ was determined using the g_mmpbsa tool[46] as follows.

$$\Delta G_{bind,PBSA} = \Delta G_{complex} - [\Delta G_{Rec} + \Delta G_{lig}]$$

$$G = E_{gas} + G_{sol} - TS$$

$$E_{gas} = E_{int} + E_{ele} + E_{vdw}$$

$$G_{sol} = G_{PB(GB)} + G_{sol-np}$$

$$G_{sol-np} = \gamma SAS$$

Where, G is Gibbs free energy, E_{gas} is the gas phase energy calculated as the sum of internal energy (E_{int}), energy generated as a result of the electrostatic interaction (E_{ele}) and the van der Waals interaction (E_{vdw}). G_{sol} is the solvation free energy calculated as the sum of polar (G_{PB}) and nonpolar contributions ($G_{sol\text{-}np}$). Polar interaction contribution (G_{PB}) was calculated as the summation of electrostatic contribution (E_{ele}) and polar solvation contribution (G_{PB}). The nonpolar solvation contribution ($G_{sol\text{-}np}$) is approximated as linearly dependent on the solvent accessible surface area (SAS) and γ is the surface tension constant that was set to 0.0072 kcal mol^{-1} Å^{-2}. Inspired by the high predicted binding affinity with tubulin compared to noscapine based on the docking score and the predictive free energy of binding using MM-PBSA, we have chemically synthesized all amido thiadiazole coupled noscapinoids for their experimental validation.

Predicted ADME Properties

A set of 44 ADME (absorption, distribution, metabolism, and excretion) properties for newly synthesized analogs of noscapine were predicted using the QikProp tool (Schrodinger package). The properties having zero values were manually deleted. The acceptability of the compounds was analyzed using Lipinski's rule of 5 (number of violations of Lipinski's rule of five) which is vital for rational drug design. When a ligand molecule violates Lipinski's rule of five, i.e., it contains more than 5 hydrogen bond donors, the molecular weight is over 500, the log P is over 5, and the total of N's and O's is over 10, poor absorption or penetration is more likely.

Cell Culture and Reagents

All the chemical reagents and culture media were obtained from Sigma. The cell lines of different tissue origins such as MCF-7 and MDAMB-231 (human breast cancer), SAOS (human osteosarcoma), h-1299 (human lung carcinoma), Hep–G2 (human liver carcinoma), HeLa (human cervical carcinoma), and HEK (human embryonic kidney normal cell lines) were obtained from the cell repository of the National Center for Cell Science Pune, Maharashtra, India. The thiadiazol coupled amide derivatives and their intermediates

were chemically synthesized. Stock solution (100 mM) of the test compounds was prepared with dimethyl sulfoxide (DMSO) and stored at 4°C until use. The cells were allowed to grow in Dulbecco's modified Eagle medium (DMEM), supplemented with 10% fetal bovine serum (FBS) and antibiotics at a temperature of 37°C under 5% CO_2 and 95% humidity. Cells with a 70–80% confluence were subcultured for bioassays using trypsin-EDTA (0.25%).

In Vitro *Cell Proliferation Assay Using Different Cell Lines*

Inhibition of cellular proliferation by the amido-thiadiazole coupled noscapinoids (**6a**–**6ac**) was carried out using five different cancer cell lines of different tissue origin and one normal cell lines. The cells were grown in a DMEM culture medium supplemented with 10% FBS, 1% penicillin/streptomycin and 2 mM l-glutamine at 37°C with 5% CO_2. Suspension cells were plated into 96-well plates at a density of 5×10^3 cells per well and were treated with gradient concentrations of noscapinoids for 72h. The harvested cells were fixed with 50% trichloroacetic acid, stained with 0.4% sulforhodamine B (dissolved in 1% acetic acid) and then washed with 1% acetic acid to remove unbound dye. The protein-bound dye was extracted with 10 mM Tris base and absorbance was measured at 564 nm using a microplate spectrophotometer. The IC_{50} values that stand for the drug concentration required to achieve a cell kill of 50% were determined using the online tool Quest GraphTM IC_{50} Calculator (AAT Bioquest, Inc., Sunnyvale, CA, USA, https://www.aatbio.com/tools/ic50-calculator).

Cellular Observation by Staining with Fluorescent Dyes

MDAMB-231 cancer cells were cultivated in 6-well plates on poly-L-lysine-coated coverslips and treated with the IC_{50} concentration of the most potent noscapinoid **6aa** for 72 h. After incubation, coverslips were removed, fixed in cold methanol and washed with PBS. It was then stained with a 10 μM concentration of DAPI, Hoechst 33342, acridine orange and ethidium bromide dye separately for 15 min at room temperature. The stained cells were washed twice in PBS and viewed using a Nikon Eclipse Ts2R-FL inverted fluorescent microscope with standard excitation filters. The excitation and emission wavelengths were 346 nm and 460 nm, respectively. Apoptotic cells in the presence of test compounds were identified by changes in morphological features (e.g., nuclear condensation, formation of membrane blebs and apoptotic bodies) compared to untreated cells.

Measurement of Mitochondrial Membrane Potential ($\Delta\Psi m$)

The effect of Noscapinoid **6aa** on mitochondrial membrane potential was measured by using three different dyes such as rhodamine-123 (Sigma-Aldrich Co.; Ex/Em = 485 nm/535 nm), JC-1 (Invitrogen Co.; Ex/Em = 515 nm/529 nm) and DAPI (Sigma-Aldrich Co.; Ex/Em = 358 nm/461 nm). Briefly, cells were seeded in 12 well plates followed by treatment with IC_{50} concentration of **6aa** for 48 h. Cells were washed with PBS and stained with rhodamine-123 (15 μg/ml), JC-1 (10 μg/ml) and DAPI (10 μg/ml) for 10 min at room temperature. After staining, cells were washed twice with PBS and images were captured using an inverted fluorescence microscope (Nikon Eclipse Ts2R-FL) at 400x magnification. The untreated cells stained with rhodamine-123 appeared light green fluorescence (lower $\Delta\Psi$m) whereas the treated cells appeared bright green fluorescence (higher $\Delta\Psi$m). In the case of JC-1 stain, light red fluorescence (lower $\Delta\Psi$m) was detected in untreated cells, whereas bright red fluorescence (higher $\Delta\Psi$m) was observed in treated cells. Similarly, in DAPI stain relatively light blue with no morphological changes was observed in untreated cells, whereas bright blue with changes in morphological features was observed in treated cells. The intensity was measured using Image J software.

Intracellular Reactive Oxygen Species (ROS) Detection

An increase in intracellular ROS induces apoptosis in cancer cells. The intracellular ROS concentration was analyzed through the oxidative conversion of the sensitive fluorescent probe 2′,7′-dichlorofluorescence-diacetate (DCFH-DA) to fluorescent 2′,7′-dichlorofluorescein (DCF). Briefly, MDAMB-231 cells were seeded in 6 well plates containing cover glass and treated with IC_{50} concentration of **6aa** for 48 h. The treated cells were harvested, washed twice with PBS, resuspended in 500 μL of 10 μM DCFH-DA (purchased from Molecular Probes Inc., Invitrogen) and incubated at room temperature for 30 min in the dark. The stained cells were observed under a fluorescent microscope (Nikon Eclipse Ts2R-FL) with standard excitation filters (Nikon).

Chemistry

General

All the solvents and reagents used are analytically pure. All the reactions were performed in oven-dried flasks with magnetic stirring. Progress of reactions was monitored by thin layer chromatography (TLC) performed on Merck 60 F-254 silica gel pre-coated plates. The TLC plates after elution were visualized illuminating at 254 nm for UV active materials. PMA staining and charring on a hot plate achieved further visualization. Column chromatography was performed using columns packed with a slurry of silica gel (200 mesh) in hexane and equilibrated with the appropriate solvent mixture. Compounds were loaded as a concentrated solution or neat and eluted with an appropriate solvent system applying pressure with an air pump. Yields refer to chromatographically and spectroscopically pure homogeneous materials unless otherwise stated. Appropriate names for all the new compounds were given with the help of Chem Draw professional 2019. Melting points were determined by CINTEX programmable melting point apparatus and are uncorrected. ^{1}H and ^{13}C-NMR spectra of samples were recorded on AVANCE- 300 MHz, 400 MHz and 500 MHz spectrometers in $CDCl_3$. Chemical shifts (δ) are described relative to TMS ($\delta = 0.0$) as the internal standard. Spin multiplicities are described as s (singlet), br. s (broad singlet), d (doublet), t (triplet), q (quartet), or m (multiplet) and coupling constants are reported in hertz (Hz). Mass spectra were recorded in ESI spectrometers. All high-resolution mass spectra were recorded on a QSTAR XL hybrid ms/ms system (Applied Biosystems/MDS sciex, foster city, USA), equipped with an ESI source (IICT, Hyderabad). Natural α-noscapine was purchased from Sigma-Aldrich and is used as such.

Procedure for the Synthesis of 7-Hydroxy-6-methoxy-3-(4-methoxy-6-methyl-5,6,7,8-tetrahydro[1,3]dioxolo-[4,5-g]isoquinolin-5-yl)isobenzofuran-1(3H)-one (**2**)

Natural noscapine **1** (2.0 g, 4.84 mmol), was dissolved in anhydrous DMF (5.0 mL) followed by the addition of sodium azide (0.63 g, 9.68 mmol) and sodium iodide (0.36 g, 2.42 mmol). The mixture was stirred vigorously for 4 h at 140 °C. The mixture was concentrated under reduced pressure to yield a dark residue which was dissolved in AcOEt (50 mL). The insoluble material was filtered through celite and the filtrate was diluted with AcOEt (50 mL) followed by washing with water (2× 25 mL) and brine (2×25 mL). The organic layer was dried over Na_2SO_4 and concentrated under reduced pressure to give the crude product which was crystallized from methanol. Product **2** was isolated as a white solid. (78% yield): m.p.: 142–143 °C; ^{1}H-NMR ((D_6)DMSO, 400 MHz): δ 9.73 (s, 1H), 7.11 (d, $J = 8.0$, 1H), 6.47 (s, 1H), 6.01 (m, 2H), 5.81 (d, $J = 8.0$, 1H), 5.48 (d, $J = 4.0$, 1H), 4.24 (d, $J = 4.0$, 1H), 3.96 (s, 3H), 3.79 (s, 3H), 2.48–2.34 (m, 2H) 2.43 (s, 3H), 2.31–2.18 (m, 1H), 1.95–1.83 (m, 1H); ^{13}C-NMR ($CDCl_3$, 100 MHz): δ 171.71, 148.44, 146.72, 144.96, 140.40, 139.17, 133.99, 132.28, 117.94, 116.61, 114.14, 113.75, 102.29, 100.76, 83.84, 60.68, 59.40, 56.72, 50.14, 46.46, 28.19; MS (ESI) *m/z* 400 $[M+H]^+$; HRMS (ESI) Calcd for $C_{21}H_{21}NO_7$ $[M+H]^+$: 400.1396, found: 400.1382.

Procedure for the Synthesis of 7-(4-Bromobutoxy)-6-methoxy-3-(4-methoxy-6-methyl-5,6,7,8-tetrahydro-[1,3]dioxolo[4,5-g]isoquinolin-5-yl)isobenzofuran-1(3H)-one (**3**)

To the solution of 7-hydroxy-6-methoxy-3-(4-methoxy-6-methyl-5,6,7,8-tetrahydro-[1,3]dioxolo[4,5-g]isoquinolin-5-yl)isobenzofuran-1(3*H*)-one (**2**, 1.0 g, 2.50 mmol) in acetone (10 mL), was added potassium carbonate (0.69 g, 5.0 mmol), potassium iodide (0.83 g, 5.0 mmol) and 1,4-dibromobutane (0.37 g, 3.75 mmol) and stirred at room temperature for 4 h. Crude reaction mixture was filtered, the filtrate was evaporated under vacuum, It was then extracted with ethyl acetate (3×50 ml), dried with anhydrous Na_2SO_4, and evaporated under reduced pressure. The desired product was isolated by usual column chromatography with a mixture of ethyl acetate and hexane (7:3) as eluents to yield **3** as a White solid, yield: 92%; m.p.:125–127 °C; ^{1}H-NMR (400 MHz, $CDCl_3$): $\delta = 6.94$ (d, $J = 8.24$, 1H), 6.30 (s, 1H), 6.05 (d, $J = 8.24$, 1H), 5.94 (dd, $J = 1.52$, 5.18, 2H), 5.57 (d, $J = 4.12$, 1H), 4.39 (d, $J = 4.12$, 1H), 4.32–4.20 (m, 2H), 4.04 (s, 3H), 3.85 (s, 3H), 3.54 (t $J = 6.71$, 2H, 2.62–2.56 (m, 1H), 2.54 (s, 3H), 2.39–2.29 (m, 2H), 2.11–2.10 (m, 2H), 1.99–1.84(m, 3H). ^{13}C-NMR (100 MHz, $CDCl_3$): $\delta = 168.10$, 152.47, 148.35, 146.50, 140.98, 140.42, 134.00, 132.12, 120.66, 118.03, 117.81, 117.07, 102.29, 100.74, 81.75, 73.51, 60.79, 59.39, 56.73, 50.02, 46.35, 34.05, 29.15, 28.62, 28.08; MS (ESI): *m/z* 534 $[M+H]^+$; HRMS (ESI): *m/z* $[M+H]^+$ Calcd for $C_{25}H_{29}BrNO_7$: 534.11066; found: 534.11219.

Procedure for the Synthesis of 7-(4-((5-Amino-1,3,4-thiadiazol-2-yl)thio)butoxy)-6-methoxy-3-(4-methoxy-6-methyl-5,6,7,8-tetrahydro-[1,3]dioxolo [4,5-g]isoquinolin-5-yl)isobenzofuran-1(3H)-one (**4**)

To the solution of 7-(4-bromobutoxy)-6-methoxy-3-(4-methoxy-6-methyl-5,6,7,8-tetrahydro-[1,3]dioxolo[4,5-g]isoquinolin-5-yl)isobenzofuran-1(3*H*)-one (**3**, 1.0 g, 1.87 mmol) in DMF (10 mL), was added potassium carbonate (0.41 g, 3.0 mmol), and 5-amino-1,3,4-thiadiazole-2-thiol (0.34 g, 2.62 mmol) and stirred at 80 °C for 2 h. The completion of the reaction was monitored by TLC checking. After completion of the reaction, the mixture was cooled to room temperature and diluted with cold water. It was then extracted with ethyl acetate (3×50 ml), dried with anhydrous Na_2SO_4, and evaporated under reduced pressure. The desired product was isolated by usual column chromatography with a mixture of ethyl acetate and hexane (2:3) as eluents to yield **4** as Yellow solid, yield: 82%; m.p.:100–102 °C; ^{1}H-NMR (500 MHz, $CDCl_3$): δ = 6.95 (d, *J* = 8.24, 1H), 6.31 (s, 1H), 6.08 (d, *J* = 8.24, 1H), 5.93 (d, *J* = 4.57, 2H), 5.59 (d, *J* = 3.81, 1H), 4.40 (d, *J* = 3.81, 1H), 4.30–4.18 (m, 2H), 4.02 (s, 3H), 3.83 (s, 3H), 3.27–3.17 (m, 2H), 2.69–2.45 (m, 4H), 2.43–2.30 (m, 2H), 2.09–1.86(m, 5H). ^{13}C-NMR (100 MHz, $CDCl_3$): δ = 168.66, 168.21, 154.82, 152.45, 148.36, 146.49, 140.90, 140.39, 133.97, 132.02, 120.48, 118.08, 117.78, 116.89, 102.30, 100.73, 81.70, 73.89, 60.76, 59.37, 56.70, 49.83, 46.18, 34.70, 28.90, 27.83, 25.80; MS (ESI): *m/z* 587 $[M+H]^+$; HRMS (ESI): *m/z* $[M+H]^+$ calc. for $C_{27}H_{31}N_4O_7S_2$: 587.16102; found: 587.16287.

General Procedure for the Synthesis of Noscapine Derivatives (**6a**–**6ac**)

The amine **2** (0.3g, 1.0 eq) obtained from the previous step was taken in an RBF (50 mL) and dissolved in DCM (10 mL). The contents were charged with EDC.HCl (1.5 eq), HOBt (1.5 eq) and corresponding acids (1.2 eq) followed by Et_3N (0.5 eq) and stirred overnight at 50 °C. After the completion of the reaction (monitored by TLC), the contents were washed with water and the organic layer was dried over anhydrous Na_2SO_4. The crude residue obtained after solvent evaporation was chromatographed over a silica gel column using hexane and ethyl acetate (2:3) to obtain the pure products as solids in good yields (for the yields and physiochemical data of compounds **6a**–**6ac**, please see the *Supporting Information*).

Acknowledgements

Authors thank ICMR (GAP-0829) for financial support. RKP thank DST for inspire-SRF (GAP-0735). CSIR-IICT communication number IICT/Pubs./2022/238

Conflict of Interest

The authors declare no conflict of interest.

Data Availability Statement

The data that support the findings of this study are available in the supplementary material of this article.

References

[1] J. U. Rasool, K. B. Mir, M. Shaikh, A. H. Bhat, Y. Nalli, A. Khalid, S. M. Ahmad, A. Goswami, A. Ali, *Bioorg. Chem.* **2022**, *122*, 105694.
[2] D. S. Shewach, R. D. Kuchta, *Chem. Rev.* **2009**, *109*, 2859–2861.
[3] J. Kleeff, M. Korc, M. Apte, C. La Vecchia, C. D. Johnson, A. V. Biankin, R. E. Neale, M. Tempero, D. A. Tuveson, R. H. Hruban, J. P. Neoptolemos, *Nat. Rev. Dis. Prim.* **2016**, *2*, 16022.
[4] E.-Y. Ko, A. Moon, *J. Cancer Prev.* **2015**, *20*, 223–231.
[5] A. DeBono, B. Capuano, P. J. Scammells, *J. Med. Chem.* **2015**, *58*, 5699–5727.
[6] M. Mahmoudian, P. Rahimi-Moghaddam, *Recent Pat. Anti-Cancer Drug Discovery* **2009**, *4*, 92–97.
[7] R. Aneja, N. Dhiman, J. Idnani, A. Awasthi, S. K. Arora, R. Chandra, H. C. Joshi, *Cancer Chemother. Pharmacol.* **2007**, *60*, 831–839.
[8] K. Ye, Y. Ke, N. Keshava, J. Shanks, J. A. Kapp, R. R. Tekmal, J. Petros, H. C. Joshi, *Proc. Natl. Acad. Sci. USA* **1998**, *95*, 1601–1606.
[9] Y. Ke, K. Ye, H. E. Grossniklaus, D. R. Archer, H. C. Joshi, J. A. Kapp, *Cancer Immunol. Immunother.* **2000**, *49*, 217–225.
[10] K. Ye, J. Zhou, J. W. Landen, E. M. Bradbury, H. C. Joshi, *J. Biol. Chem.* **2001**, *276*, 46697–46700.
[11] E. K. Rowinsky, *Annu. Rev. Med.* **1997**, *48*, 353–374.
[12] J. Zhou, P. Giannakakou, *Curr. Med. Chem. Anti-Cancer Agents* **2005**, *5*, 65–71.
[13] C. Theiss, K. Meller, *Cell Tissue Res.* **2000**, *299*, 213–224.
[14] K. S. Topp, K. D. Tanner, J. D. Levine, *J. Comp. Neurol.* **2000**, *424*, 563–576.
[15] J. W. Landen, R. Lang, S. J. McMahon, N. M. Rusan, A.-M. Yvon, A. W. Adams, M. D. Sorcinelli, R. Campbell, P. Bonaccorsi, J. C. Ansel, D. R. Archer, P. Wadsworth, C. A. Armstrong, H. C. Joshi, *Cancer Res.* **2002**, *62*, 4109–4114.
[16] J. Zhou, M. Liu, R. Aneja, R. Chandra, H. Lage, H. C. Joshi, *Cancer Res.* **2006**, *66*, 445–452.
[17] J. Zhou, D. Panda, J. W. Landen, L. Wilson, H. C. Joshi, *J. Biol. Chem.* **2002**, *277*, 17200–17208.

[18] B. Dahlström, T. Mellstrand, C. G. Löfdahl, M. Johansson, *Eur. J. Clin. Pharmacol.* **1982**, *22*, 535–539.
[19] A. J. DeBono, J. H. Xie, S. Ventura, C. W. Pouton, B. Capuano, P. J. Scammells, *ChemMedChem* **2012**, *7*, 2122–2133.
[20] A. J. Debono, S. J. Mistry, J. Xie, D. Muthiah, J. Phillips, S. Ventura, R. Callaghan, C. W. Pouton, B. Capuano, P. J. Scammells, *ChemMedChem* **2014**, *9*, 399–410.
[21] P. E. Ghaly, C. D. M. Churchill, R. M. Abou El-Magd, Z. Hájková, P. Dráber, F. G. West, J. A. Tuszynski, *Can. J. Chem.* **2017**, *95*, 649–655.
[22] N. K. Manchukonda, B. Sridhar, P. K. Naik, H. C. Joshi, S. Kantevari, *Bioorg. Med. Chem. Lett.* **2012**, *22*, 2983–2987.
[23] N. K. Manchukonda, P. K. Naik, S. Santoshi, M. Lopus, S. Joseph, B. Sridhar, S. Kantevari, *PLoS One* **2013**, *8*, e77970.
[24] N. K. Manchukonda, P. K. R. Nagireddy, B. Sridhar, S. Kantevari, *Res. Chem. Intermed.* **2017**, *43*, 2457–2469.
[25] P. K. R. Nagireddy, V. K. Kommalapati, V. Siva Krishna, D. Sriram, A. D. Tangutur, S. Kantevari, *ACS Omega* **2019**, *4*, 19382–19398.
[26] S. Santoshi, N. K. Manchukonda, C. Suri, M. Sharma, B. Sridhar, S. Joseph, M. Lopus, S. Kantevari, I. Baitharu, P. K. Naik, *J. Comput.-Aided Mol. Des.* **2015**, *29*, 249–270.
[27] Y. Li, J. Geng, Y. Liu, S. Yu, G. Zhao, *ChemMedChem* **2013**, *8*, 27–41.
[28] D. Kumar, N. Maruthi Kumar, K.-H. Chang, K. Shah, *Eur. J. Med. Chem.* **2010**, *45*, 4664–4668.
[29] D. Kumar, B. R. Vaddula, K.-H. Chang, K. Shah, *Bioorg. Med. Chem. Lett.* **2011**, *21*, 2320–2323.
[30] X.-W. Kong, Y.-H. Zhang, T. Wang, Y.-S. Lai, S.-X. Peng, *Chem. Biodiversity* **2008**, *5*, 1743–1752.
[31] R. C. Mishra, P. Karna, S. R. Gundala, V. Pannu, R. A. Stanton, K. K. Gupta, M. H. Robinson, M. Lopus, L. Wilson, M. Henary, R. Aneja, *Biochem. Pharmacol.* **2011**, *82*, 110–121.
[32] R. Aneja, S. N. Vangapandu, M. Lopus, R. Chandra, D. Panda, H. C. Joshi, *Mol. Pharmacol.* **2006**, *69*, 1801–1809.
[33] P. K. Naik, M. Lopus, R. Aneja, S. N. Vangapandu, H. C. Joshi, *J. Comput.-Aided Mol. Des.* **2012**, *26*, 233–247.
[34] R. Aneja, S. N. Vangapandu, M. Lopus, V. G. Viswesarappa, N. Dhiman, A. Verma, R. Chandra, D. Panda, H. C. Joshi, *Biochem. Pharmacol.* **2006**, *72*, 415–426.
[35] M. A. Oliva, A. E. Prota, J. Rodríguez-Salarichs, Y. L. Bennani, J. Jiménez-Barbero, K. Bargsten, Á. Canales, M. O. Steinmetz, J. F. Díaz, *J. Med. Chem.* **2020**, *63*, 8495–8501.
[36] R. A. Friesner, J. L. Banks, R. B. Murphy, T. A. Halgren, J. J. Klicic, D. T. Mainz, M. P. Repasky, E. H. Knoll, M. Shelley, J. K. Perry, D. E. Shaw, P. Francis, P. S. Shenkin, *J. Med. Chem.* **2004**, *47*, 1739–1749.
[37] T. A. Halgren, R. B. Murphy, R. A. Friesner, H. S. Beard, L. L. Frye, W. T. Pollard, J. L. Banks, *J. Med. Chem.* **2004**, *47*, 1750–1759.
[38] P. K. Naik, B. P. Chatterji, S. N. Vangapandu, R. Aneja, R. Chandra, S. Kanteveri, H. C. Joshi, *J. Comput.-Aided Mol. Des.* **2011**, *25*, 443–454.
[39] M. J. Abraham, T. Murtola, R. Schulz, S. Páll, J. C. Smith, B. Hess, E. Lindahl, *SoftwareX* **2015**, *1–2*, 19–25.
[40] V. Hornak, R. Abel, A. Okur, B. Strockbine, A. Roitberg, C. Simmerling, *Proteins* **2006**, *65*, 712–725.
[41] J. Wang, R. M. Wolf, J. W. Caldwell, P. A. Kollman, D. A. Case, *J. Comput. Chem.* **2004**, *25*, 1157–1174.
[42] A. Jakalian, D. B. Jack, C. I. Bayly, *J. Comput. Chem.* **2002**, *23*, 1623–1641.
[43] A. W. Sousa da Silva, W. F. Vranken, *BMC Res. Notes* **2012**, *5*, 367.
[44] J. P. Ryckaert, G. Ciccotti, H. J. C. Berendsen, *J. Comput. Phys.* **1977**, *23*, 327–341.
[45] P. A. Kollman, I. Massova, C. Reyes, B. Kuhn, S. Huo, L. Chong, M. Lee, T. Lee, Y. Duan, W. Wang, O. Donini, P. Cieplak, J. Srinivasan, D. A. Case, T. E. Cheatham 3rd, *Acc. Chem. Res.* **2000**, *33*, 889–897.
[46] R. Kumari, R. Kumar, A. Lynn, *J. Chem. Inf. Model.* **2014**, *54*, 1951–1962.

Received November 18, 2022
Accepted January 3, 2023

